THE EFFECT OF TEMPERING TEMPERATURE ON MICROSTRUCTURE AND WEAR BEHAVIOR OF TUNGSTEN AND BORON ALLOYED Ni-HARD 4 WHITE CAST IRONS

Burak Barutçuoğlu
Department of Metallurgical and Materials Engineering, Kocaeli University, Kocaeli, Turkey
ONATUS Vision Technologies, Kocaeli, Turkey

Funda Gül Koç and Ersoy Erişir
Department of Metallurgical and Materials Engineering, Kocaeli University, Kocaeli, Turkey

Gülben Karaarslan
Department of Metallurgical and Materials Engineering, Kocaeli University, Kocaeli, Turkey
ONAT Aluminum, Kocaeli, Turkey

Copyright © 2024 The Author(s)
https://doi.org/10.1007/s40962-024-01322-8

Abstract

This study investigates the effect of tempering temperature on the microstructure and wear resistance of high-alloy white cast iron (Ni-Hard 4) with 1.15% W and 0.5% B additions. Specimens were austenitized at 850 °C for 5 h, quenched in air, and tempered at temperatures between 250 and 650 °C for 4 h. Equilibrium and non-equilibrium thermodynamic calculations were performed using Thermo-Calc software. After the microstructural investigations, hardness testing was carried out. A pin-on-disk tribometer was used to conduct wear tests under dry sliding conditions. Microstructure and worn surfaces were examined using light and scanning electron microscopes. The results showed that increasing tempering temperature resulted in a higher volume fraction of carbides. It was found that tempering at 550 °C for four hours increases resistance to wear giving the lowest measured values of weight loss and wear rate. Accordingly, tempering allows the precipitation of fine carbides in the martensitic matrix which may increase wear resistance.

Keywords: *Ni-Hard 4, tungsten, boron, heat treatment, microstructure, wear, white cast iron, WCI*

Introduction

High-alloyed white cast iron (WCI) is widely used in several industrial fields, such as mining, cement, paper, copper, and steel manufacturing, due to its high wear resistance.[1–6] According to ASTM A532, Ni-Hard 4 is a WCI alloy containing approximately 3% C, 8–10% Cr, and 4–6% Ni by weight.[7] Despite its higher alloy costs, Ni-Hard 4 offers higher strength and toughness, making it an ideal choice for heavy-duty applications, such as crushing and grinding.[8]

In as-cast condition, Ni-Hard 4 alloy exhibits a microstructure comprising eutectic M_7C_3 carbides dispersed within a predominantly austenitic matrix, but predominantly martensitic after hardening and tempering.[9] Generally, the hardness is dependent on the chemical composition, matrix type, and retained austenite amount as well as the type, volume fraction, and distribution of carbides.[10,11] M_7C_3-type primary and eutectic carbides can be found in lamellar morphology (rod or blade-like) with austenitic matrix. The hexagonal carbide of M_7C_3-type contains approximately equal amounts of chromium, iron, and other potential carbide former elements.[12] Furthermore, it can dissolve up to 2.8% boron.[13] Depending on the iron content, the hardness values of M_7C_3 can be relatively low and vary from 1190 to 1800 HV. It is also typical that M_7C_3 may be surrounded by an M_3C layer.[13] Apart from

Received: 05 February 2024 / Accepted: 13 March 2024
Published online: 22 April 2024

Table 1. Chemical Composition of Investigated Material in this Study (wt.%)

	C	Si	Mn	P	S	Cr	Ni	Mo	W	B
ASTM A532	2.5–3.6	≤ 2	≤ 2	≤ 0.1	≤ 0.15	7–11	4.5–7	≤ 1.5	–	–
Material	3.3	0.8	0.8	0.09	0.09	8.0	6.3	1.5	1.2	0.5

this, other primary, eutectic, and secondary carbides of $M_{23}C_6$, M_6C, M_2C, and MC are also observed.[14–16]

After the hardening and tempering treatments, the matrix is predominantly martensitic including some secondary carbides and retained austenite.[17,18] The WCI alloys are typically austenitized at temperatures between 800 and 1100 °C for usual holding times between 1 and 6 h and followed by air cooling.[19–21] When considering the austenitizing temperature, two primary hardening methods can be found: stabilizing heat treatment and destabilizing heat treatment.[20] The utilization of stabilizing heat treatment with high austenitization temperature eliminates the pearlite formed during cooling after solidification. Due to the gradual dissolution of secondary carbides at high temperatures, a quenching is required to obtain a substantial fraction of retained austenite including increased carbon and chromium content. On the other hand, the destabilizing method at lower temperatures aims to achieve a mainly martensitic matrix without dissolving secondary carbides to avoid an increased amount of retained austenite by higher carbon content.[21] After the hardening of WCI alloys, tempering, also known as subcritical heat treatment, is generally applied at temperatures between 200 and 600 °C for 2–6 h.[22] Tempering improves toughness, relieves residual stresses, and reduces the retained austenite fraction.[18,21] During the tempering, carbide-involved reactions such as secondary carbide precipitation, eutectic reaction, and pearlite formation can be formed. In general, secondary carbide precipitation is preferred because this destabilizes the retained austenite, thereby promoting the formation of martensite during the cooling.[22]

The wear resistance of WCI alloys is known to be dependent not only on the matrix microstructure but also on the carbide type and properties, such as size, morphology, distribution, and orientation.[4,9,20] Various carbide-forming elements, including Ti, V, Nb, Mo, and W can be used to modify the carbide type. Researchers[5,10,23–29] have reported a considerable increase in wear resistance by adding carbide-forming elements to WCI alloys. Si and B are added to modify the eutectic carbide structure by segregation into the matrix/carbide interphase. B is only very weakly soluble in Fe, either in austenite or in ferrite. Further additions can form borides which are harder and more thermally stable than carbides.[9,30–32] According to the literature,[10,15] the B additions in the range of 0.26–0.59 wt.% significantly increase the volume fraction of eutectic carbides, resulting in an improvement in wear resistance.

In this paper, the effect of tempering temperature on the microstructure, hardness, and wear resistance of tungsten-boron added Ni-Hard 4 has been investigated. It is aimed to determine the optimum hardness and wear resistance after hardening at 850 °C and tempering at temperatures between 250 and 650 °C. In order to explain the microstructural evolution, the CALculation of PHAse Diagrams (CALPHAD) methodology was used, and the correlation of the microstructure was performed by different characterization techniques including light microscopy (LM), scanning electron microscopy (SEM), and X-ray diffraction analysis (XRD).

Experimental Procedures

The experimental high-alloy WCI material for the present study was melted in an induction furnace with a 25 kg capacity at 1390 °C. The material was subsequently cast into a sand mold as a specimen with dimensions of $100\times180\times18$ mm^3. The chemical composition of the investigated material is given in Table 1. The material has the base composition of martensitic WCI-class I-type D designation Ni-HiCr according to ASTM A532 (also named commercially as Ni-Hard 4) but includes W and B as alloying elements.

Thermodynamic calculations were carried out with the CALPHAD methodology using the chemical composition obtained after the casting. Thermo-Calc commercial software with TCFE12 Steel and Fe-alloys thermodynamic database was used for the given chemical composition in Table 1. During the calculations, diamond, graphite, and cementite were suspended. The CALPHAD methodology provides reliable thermodynamic data in the determination of microstructure and production process parameters according to chemical composition. Thermodynamic data can be utilized to calculate various material data through calculations involving stable and metastable phases, phase components and amounts, critical transformation temperatures, and non-equilibrium solidification analysis using the Scheil–Gulliver approach.[33] The Scheil–Gulliver model examines the solidification path of an alloy under the assumption that each element segregates independently throughout the process. This implies that the alloy is

approached as a combination of individual elements rather than a homogenized solution. The model calculates the evolution of phases as temperature decreases, considering the distribution of each element between the liquid and solid phases.

For the hardening and tempering heat treatments, the specimens were cut from the material in as-cast condition. All specimens were austenitized at 850 °C for 5 h and air quenched (AQ) for the hardening. The hardened samples were tempered at five different tempering temperatures of 250, 350, 450, 550, and 650 °C for 4 h. The schematic representation of the hardening and tempering treatments is shown in Figure 1.

The metallographic specimens were ground using SiC abrasive papers after the heat treatments and polished with 3 µm diamond solution using standard metallographic procedures. The polished specimens were etched with Beraha II (800 ml H_2O, 400 ml HCl, 48 g NH_4HF_2, 1 g $K_2O_7S_2$) solution for 20 s and deep etched in a solution of 75% HCl, %24 HNO_3, %1 HF for 20 min to reveal the microstructure. The microstructural investigations of the specimens were performed using a light microscope (LM, model: OLYMPUS-BX53M) and scanning electron microscope (SEM, model: TESCAN Vega 3 XMH Chamber) with energy-dispersive X-ray spectroscopy (EDX, model: EDAX APEX). An X-ray diffractometer (XRD, model: Rigaku Ultima+) with Cu Kl (λ=1.54056 A°) radiation was used to identification of the phases observed in the microstructure investigations. 2θ-range was applied from 10° to 90°during the analysis. The MDI Jade 7.0 program and 2004 library were used to determine XRD peaks.

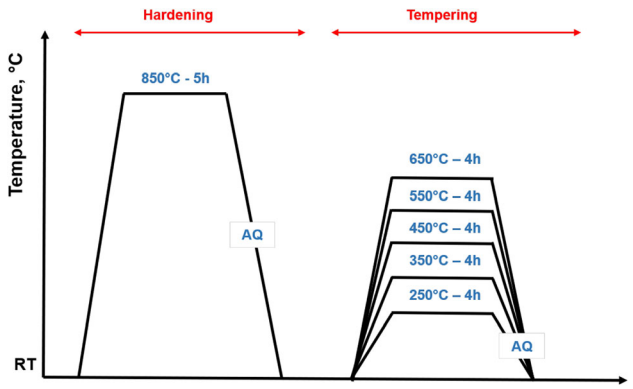


Figure 1. The schematic representation of the heat treatment process.

Hardness tests were carried out using a Vickers hardness tester (model: Future-Tech FV700) under a 20 kg load for 10 s of loading duration. The average hardness values were calculated from five measurements for each specimen.

On the specimens tempered at different temperatures, wear tests were performed to characterize the tribological behavior. Wear tests were carried out at room temperature under dry sliding conditions using a NANOVEA MT60 ball-on-disk tribometer in Figure 2 applying a normal load of 50 N. Wear testing was performed to measure the wear resistance and the friction coefficient according to ASTM G99-17[34] standard. The counter surface material was an alumina ball with a spherical geometry of 5 mm diameter as a counter surface. The sliding speed and the sliding distance were kept constant at 0.04 m s^{-1} and a distance of 250 m, respectively for all tests. Following the wear test, the worn specimens were thoroughly cleaned using ethyl alcohol to measure the wear loss by a balance with a resolution of 0.001 mg. Additionally, the worn surfaces of the

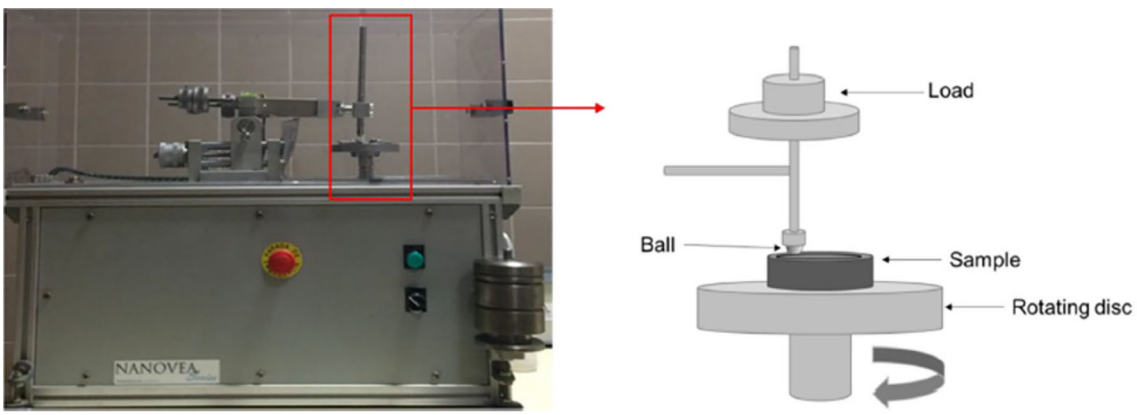


Figure 2. Experimental set-up of NANOVEA MT60 tribometer for wear testing.

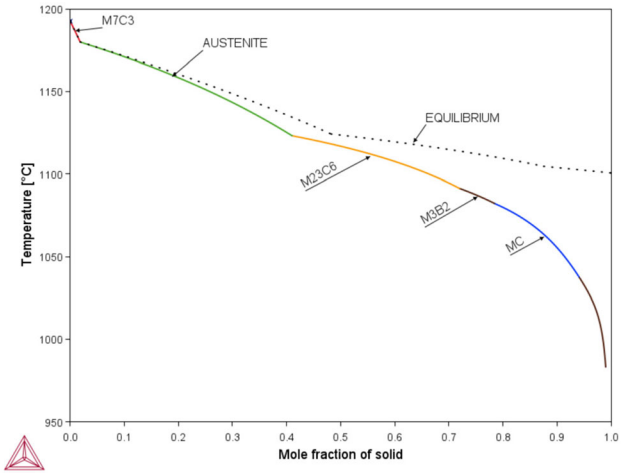


Figure 3. The temperature versus the mole fraction of solid by equilibrium (dotted line) and Scheil–Gulliver (colored-solid line) curves for Ni-Hard 4.

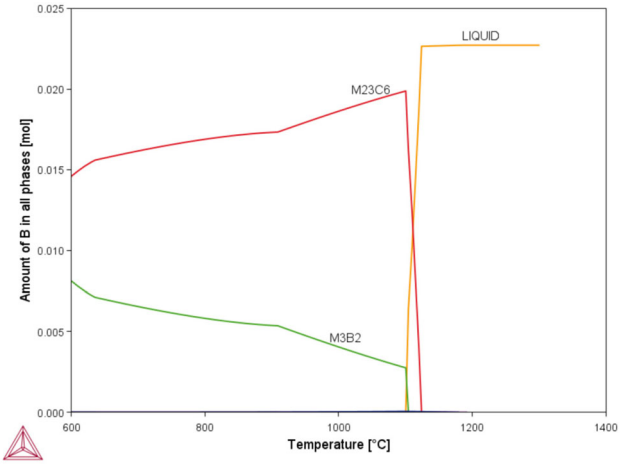


Figure 5. The amount of boron in the temperature-dependent phases of the diagram.

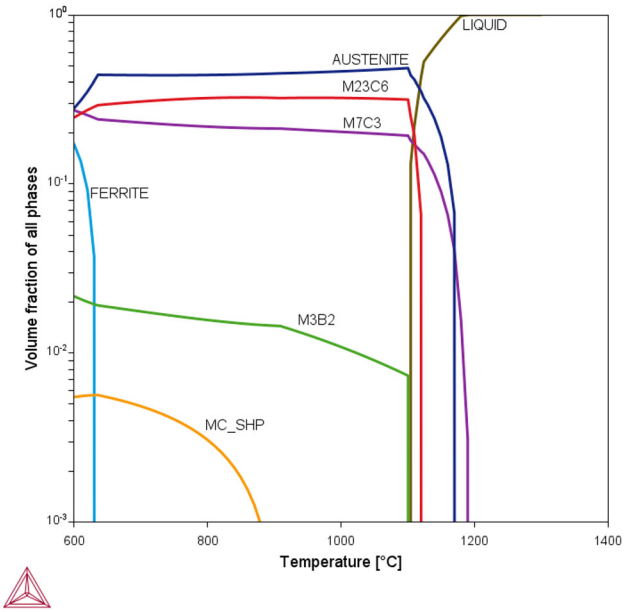


Figure 4. Calculated volume fractions of all phases for Nihard-4 as a function of temperature.

specimens were further analyzed and examined using SEM to investigate the wear mechanisms.

Results and Discussion

Thermodynamic Calculations

In order to understand the phase transformations in Ni-Hard 4 material, thermodynamic calculations were performed. The equilibrium calculations are valuable in predicting the phase compositions. However, it is essential to note that the solidification of cast alloys generally occurs under non-equilibrium conditions. Non-equilibrium solidification and equilibrium phase transformations were calculated for the chemical composition of Ni-Hard 4 material using Thermo-Calc software. Figure 3 shows the calculated mole fraction of solid as a function of temperature based on the equilibrium and the Scheil–Gulliver model for solidification. There is a large difference between liquidus temperatures calculated for equilibrium and Scheil–Gulliver non-equilibrium conditions.

According to the results predicted by the Scheil–Gulliver model, the solidification path starts with M_7C_3 precipitation before austenite (γ) formation. Besides the austenite, $M_{23}C_6$ and MC carbides and a boride (M_3B_2) are predicted. On the other hand, Figure 3 shows the dissolution of MC carbide containing W, Mo, and C at the end of the solidification. The liquidus temperature is calculated as 995.6 °C. The Scheil–Gulliver non-equilibrium solidification path can be described as:

$$\begin{aligned} &L \rightarrow L + M_7C_3 \rightarrow L + M_7C_3 + \gamma \rightarrow L + M_7C_3 \\ &+ \gamma + M_{23}C_6 \rightarrow L + M_7C_3 + \gamma + M_{23}C_6 \\ &+ \ M_3B_2 \rightarrow L + M_7C_3 + \gamma + M_{23}C_6 + M_3B_2 \\ &+ MC \rightarrow L + M_7C_3 + \gamma + M_{23}C_6 + M_3B_2. \end{aligned}$$

The equilibrium solidification displayed a different path and a narrower solidification interval as shown in Figures 3 and 4. The solidification starts with primary M_7C_3 carbide at 1193 °C and is completed at 1094 °C with the formation of austenite and $M_{23}C_6$ carbide. The equilibrium solidification path can be given as:

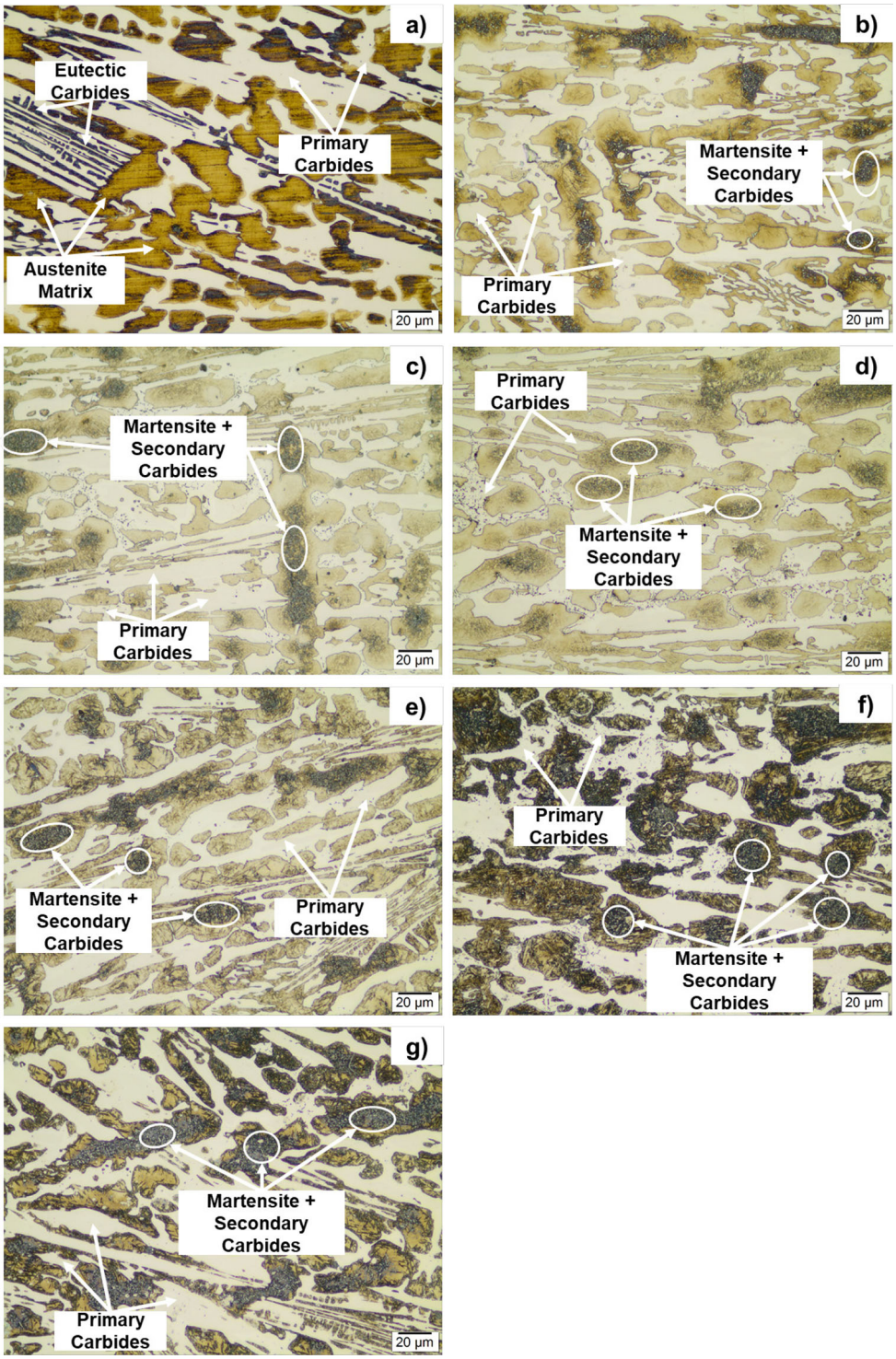


Figure 6. Light microscope images of samples (a) as-cast, (b) hardening, (c) 250 °C, (d) 350 °C, (e) 450 °C, (f) 550 °C, and (g) 650 °C.

$$L + M_7C_3 \rightarrow L + M_7C_3 + \gamma \rightarrow L + M_7C_3 + \gamma + M_{23}C_6 \rightarrow L + M_7C_3 + \gamma + M_{23}C_6 + M_3B_2.$$

Thus, both equilibrium and non-equilibrium solidification paths are completed with the same phases at the end of solidification. The equilibrium volume fractions of all phases are plotted in Figure 4. M_7C_3 carbide has a volume amount of 27.5% at 600 °C. Fe-rich $M_{23}C_6$ carbide includes C and B elements as well as some Cr. Austenite contains mostly Fe, Ni, and some Si, it has a volume of 28.1% at 600 °C. A small amount (0.542 vol.%) of MC carbide including W, Mo, and C elements is also calculated. At the equilibrium conditions, MC carbide was not calculated during the solidification, but MC phase formation is predicted below 878 °C.

The alloying elements Fe, Mo, W, and Cr may form carbides, carborides, or borides with C and B. According to previous studies,[15,31] boron segregates along prior austenite grain boundaries and then portioned to $M_{23}C_6$ carbides during the tempering process. Purba et al.[35] found that the precipitation of M_2B borides occurs during solidification prior to its transformation of $M_{23}(C,B)_6$ carborides during tempering. However, thermodynamic calculations conducted in this study indicate that M_3B_2 borides remain stable at Scheil–Gulliver non-equilibrium conditions. The calculated amount of boron in all phases is given at temperatures from 600 to 1400 °C in Figure 5. At the equilibrium conditions, it is clear that only liquid, $M_{23}C_6$, and M_3B_2 phases dissolve boron. As a boron including carbide, $M_{23}C_6$ can also be named as $M_{23}(C, B)_6$ carboride.

Microstructural Characterization

The light microscope images of samples in as-cast and tempered conditions are given in Figure 6. In as-cast condition as shown in Figure 6a, a hypoeutectic structure with primary carbides surrounded by austenite and eutectic appears in the microstructure. Light contrasted dendrites of M_7C_3 primary carbides and brownish interdendritic austenite are visible. Additionally, ledeburitic eutectic carbides can be seen in darker contrasted areas. These results are similar to the findings of previous research[36–40] on WCI alloys with a 0.5% addition of boron. They concluded that dendritic solidified austenite matrix and interdendritic structure dispersed in the form of a continuous network occurred due to boron addition.

After the hardening and tempering, the austenitic matrix transforms to martensite including secondary carbides as shown in Figure 6b–g. Increasing the tempering temperature results in a higher volume amount of secondary carbides. The phase amounts measured from the light microscope images after casting and tempering positions are given in Figure 7.

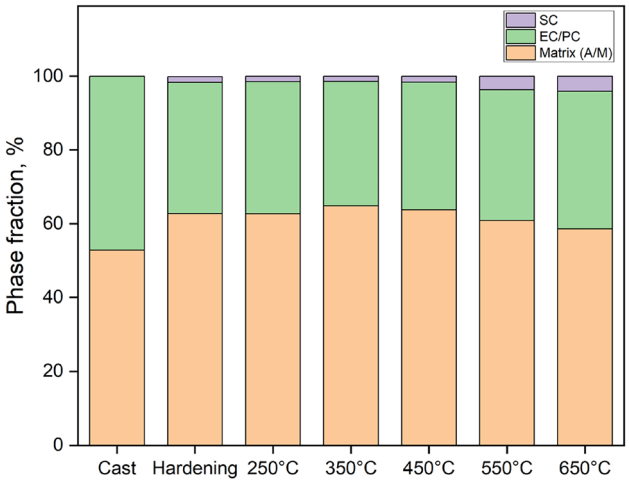


Figure 7. Phase analysis results from LM micrographs using Olympus Stream Software (SC: Secondary Carbide, EC: Eutectic Carbide, PC: Primary Carbide, and A/M: Austenite/Martensite).

Figure 8 shows SEM micrographs of the as-cast and the tempered samples. It is seen from Figure 8a that the microstructure of the as-cast sample consists of M_7C_3 primary carbides and an austenite matrix. After hardening and tempering, the microstructure is characterized by a martensitic matrix along with well-distributed secondary carbides, as revealed in Figure 8c–g. At tempering temperatures above 550 °C, the volume fraction of secondary carbides in the microstructure is increased in Figure 9. The highest secondary carbide amount is observed in the samples tempered at 550 °C and 650 °C. The volume fraction of secondary carbides fell into the range of 1.4–4.1%.

Figure 10 shows SEM secondary electron (SE) and backscattered electron (BSE) images of the sample in the as-cast condition. In general, austenite, M_7C_3, $M_{23}CB_6$, and M_2CB can be distinguished. In the SE image in Figure 10a, the contrast separation in the chromium carbides is not very clear, but in the BSE image in Figure 10b the chromium carbides coexist in M_7C_3 and $M_{23}C_6$ types. $M_{23}C_6$ type carbides form an outer shell around the M_7C_3 carbides. With the presence of boron, the formation of $M_{23}(C, B)_6$ carbide is observed, which forms an outer shell around the M_7C_3 carbides.[35,41,42]

EDX analysis was performed on the selected areas from the cast and tempered at 550 °C samples to determine the chemical compositions of carbides/carborides in the microstructure investigated (Figures 11 and 12). In the microstructure of the sample in the as-casted condition in Figure 11, EDX spot 1 analysis confirms that there are

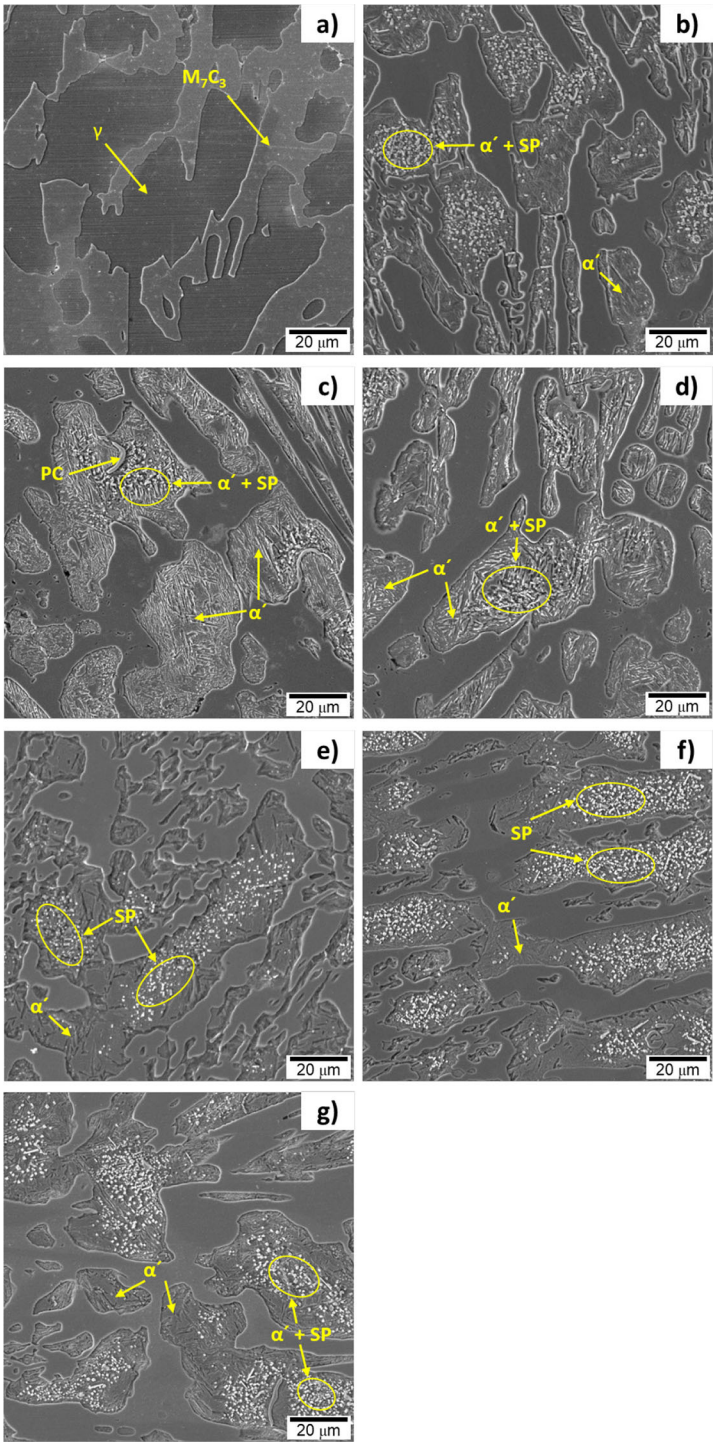


Figure 8. SEM images of samples (a) as-cast, (b) hardening, (c) 250 °C, (d) 350 °C, (e) 450 °C, (f) 550 °C and (g) 650 °C. (γ: Austenite, α′: Martensite, SP: Secondary precipitate, PC: Primary carbide).

carborides rich in tungsten and molybdenum elements. The presence of Ni, Si, and Mn elements can be seen in the matrix, as can be seen in EDX spot 2. Elemental analysis of M_7C_3 carbides is given in EDS spot 3. Some W and Mo elements were also found in chromium carbides. These elements affect the carbide type and generally make $M_{23}C_6$ type carbide. The EDX analysis of the secondary precipitates in the sample tempered at

550 °C is given in Figure 12. As seen in the EDX spot analysis on the 550 °C sample, the secondary precipitates are carbides rich in Fe and Cr elements. As seen in Figure 12, the morphology of the secondary carbides can be in the form of a cube, discrete-rod or plate-like shapes, as noted by Ruangchi et al.[43] The morphology of primary, eutectic, and secondary carbides of deep-etched samples is shown in Figure 13, in which Figure 13a–c are images of the samples in as-cast condition, and Figure 13d–f are of the tempered sample. Microstructure

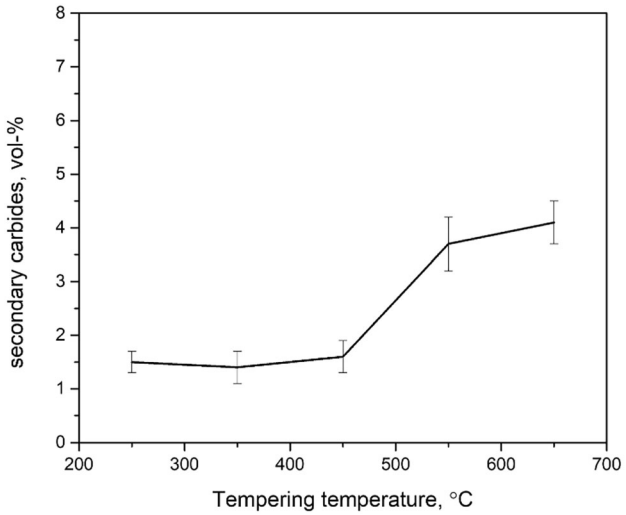


Figure 9. Volume amounts of secondary carbides measured from SEM images.

in the as-cast condition is characterized by primary and eutectic carbides. M_2(C, B) is also visible in Figure 13c. It was also seen that some cracks are found in the primary carbide. In the tempered sample, secondary carbides appeared deeply etched matrix areas as indicated in Figure 13f.

In as-cast and tempered at 550 °C samples, EDX element mapping analyses taken from primary carbide, secondary carbides, and matrix are presented in Figure 14. As can be seen on the mapping of the as-cast sample, the Fe and Ni are mainly distributed in the alloy matrix. Primary carbides, on the other hand, show the presence of Cr, C and, some Mo. In addition, M_2C type carbide with Mo and W is seen. In the EDX analysis performed on the sample tempered at 550 °C, the presence of Fe and Ni elements in the martensite matrix is observed. M_7C_3, $M_{23}C_6$ and, secondary carbides contain Cr, C and, some Mo elements. Boron could not be detected in the mapping analysis.

Figure 15 shows the XRD patterns of the samples in as-cast and tempered conditions. The sample in as-cast condition mainly consists of austenite matrix (γ-Fe) and chromium carbides of M_7C_3 and $M_{23}C_6$. After hardening, the austenite matrix transformed into the martensitic matrix. It is seen that there is some austenite and secondary carbides in the structure after the hardening. The XRD spectrums of tempered samples show α-Fe, M_7C_3, $M_{23}C_6$ and M_2C phases. Although the matrix turned into martensite with hardening and tempering, XRD spectrums show the presence of retained austenite in the

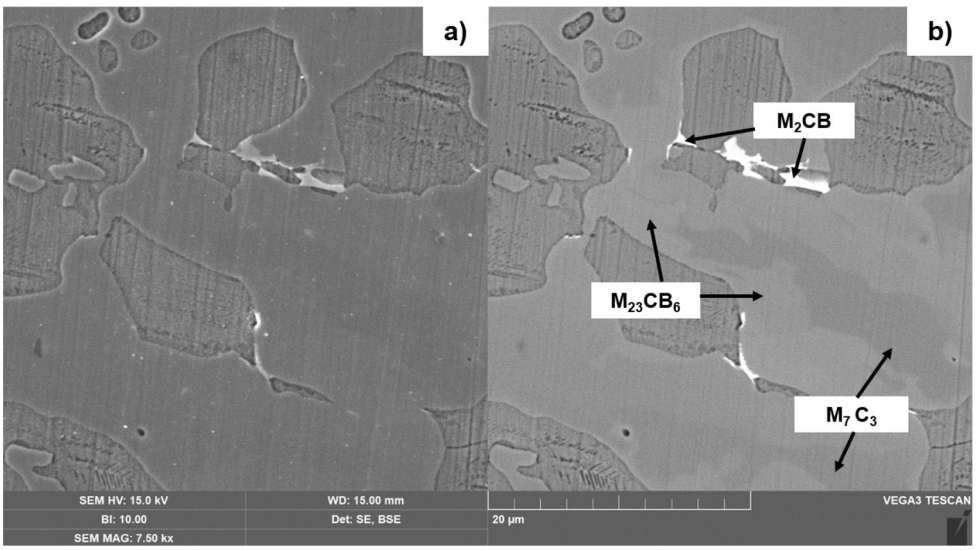


Figure 10. SEM micrographs of the sample in as-cast condition in (a) SE and (b) BSE modes.

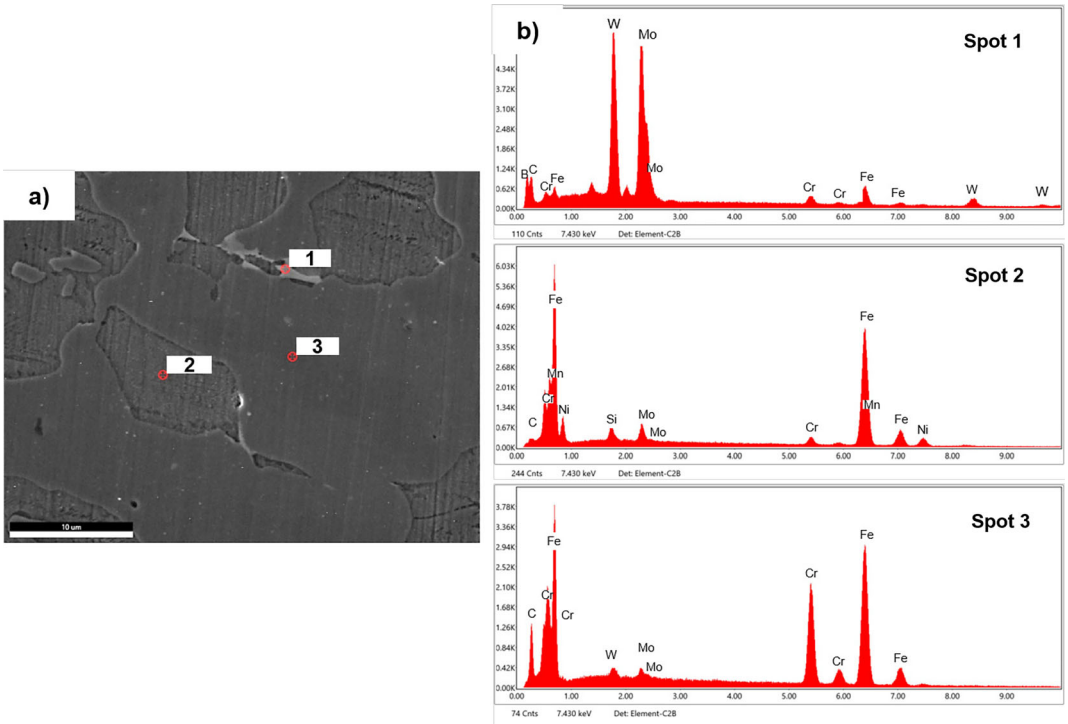


Figure 11. Microstructure of the sample in as-cast condition; (a) SEM micrograph and (b) EDX analysis.

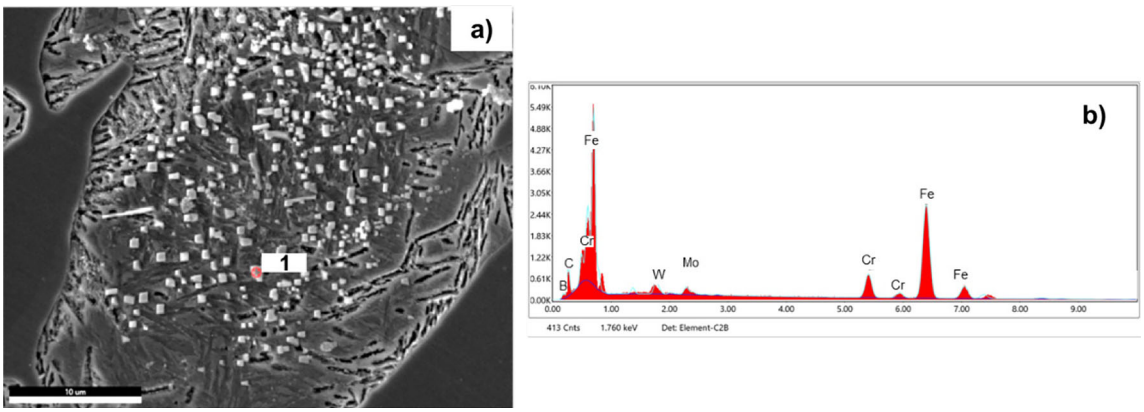


Figure 12. Microstructure of the sample tempered at 550 °C; (a) SEM micrograph, (b) EDX analysis.

tempered samples. Retained austenite was eliminated partially by tempering.

Hardness

Hardness tests were performed to determine the effect of tempering temperatures on the hardness of materials. The hardness results are given in Figure 16. It is observed that the hardness values generally increase with increasing tempering temperature. In as-casted condition, the casting hardness of Ni-Hard 4 WCI materials with the austenitic matrix is between 442 and 556 HV according to the literature.[44] In the as-casted condition, the hardness was measured at 529±13 HV which is in this range. On the other hand, the hardness increases after the hardening and tempering as expected. Hardness values were measured between 555 and 700 HV depending on the tempering temperatures from 250 to 650 °C. It can be concluded that the transformation matrix from austenite to martensite and precipitation of secondary carbides and carborides. Figure 16 indicates also that increasing the tempering

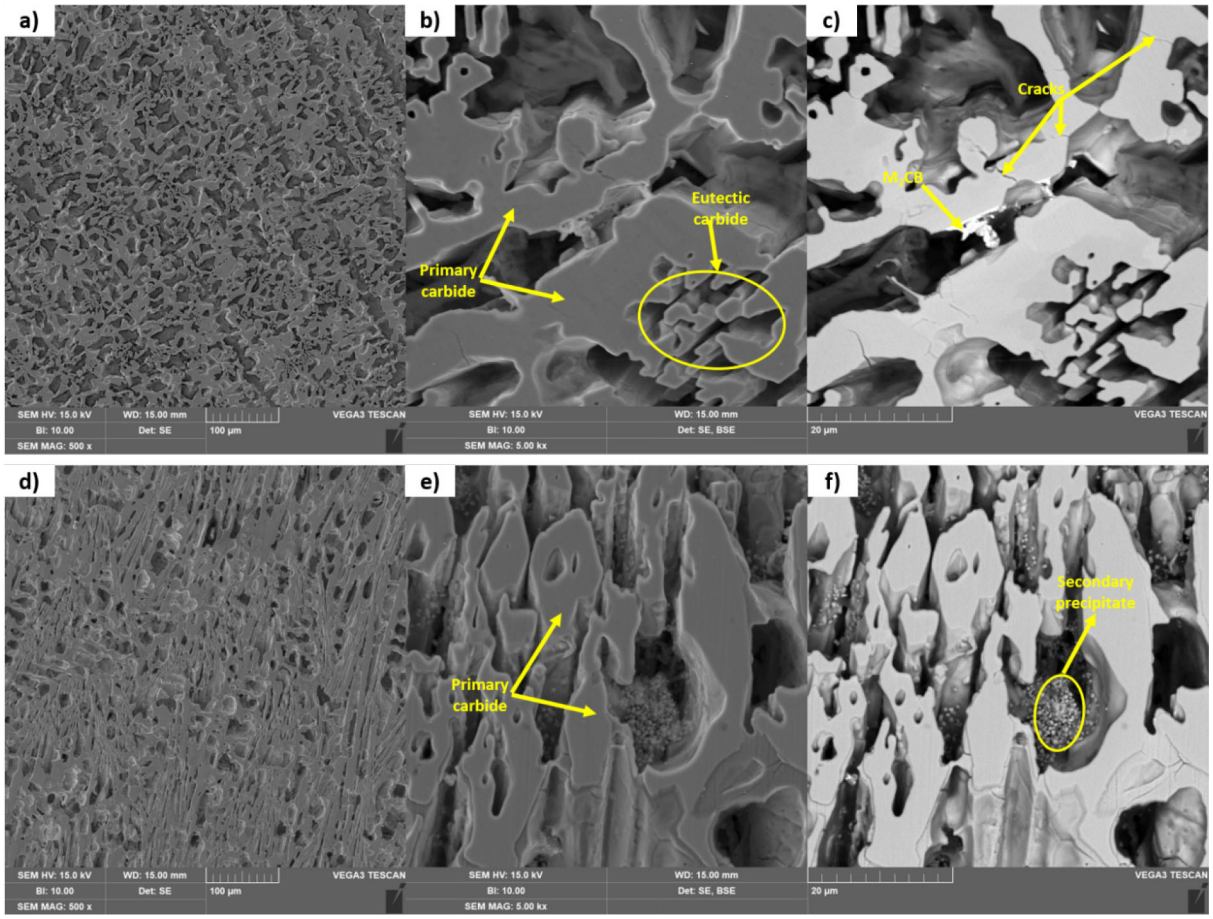


Figure 13. SEM image of deep etched as-cast (a) eutectic solidification structure, (b) SE-high magnification, (c) BSE-high magnification and tempered at 550 °C (d) eutectic solidification structure, (e) SE-high magnification, (f) BSE-high magnification.

temperature has a noticeable effect on hardness, resulting in an upward trend. It may be due to the rise in tempering temperature leading to an increase in the volume fraction of secondary precipitates within the structure. These results are comparable to the volume amounts of secondary carbide in Figure 8. The highest hardness value was measured in the sample tempered at 550 °C. The observed slight decrease in hardness could potentially be attributed to the coarsening of secondary precipitates in the sample tempered at 650 °C. As it is known, between 500 and 650 °C is the range in which secondary hardness occurs in iron-based alloys. As can be seen from the hardness measurements, the hardness increased even more with the tempering processes performed at 550 and 650 °C after hardening.

Wear Characterization

Figure 17 compares the wear testing results of the samples in the as-cast and tempered conditions. It is clear from Figure 17a that the weight loss and wear rate values are low after the tempering. In the as-cast condition, the negative effect of the austenitic matrix on the wear resistance of the specimen is clearly visible. A softer matrix provides less support to the hard carbide phases.[41] As the tempering temperature changes, the lowest average values of weight loss and wear rate are measured for the sample tempered at 550 °C, which has the highest hardness. As is known, this temperature is the secondary hardness temperature. Despite the hardness value of the sample tempered at 650 °C being the highest, the size of the secondary carbides increased significantly in the wear rate, as it is the carbide coarsening temperature. The sample with the second-best wear rate is tempered at 250 °C. Compared to 550 °C, there is a difference of approximately 100 HV in their hardness. The wear rate standard deviation is also high. Since 250 °C is the typical stress relief temperature, the sample tempered at 550 °C has a better wear rate than other tempering temperatures and the cast sample. The formation of secondary precipitates and martensite matrix with tempering provides an improvement in the wear rate compared to the cast sample.

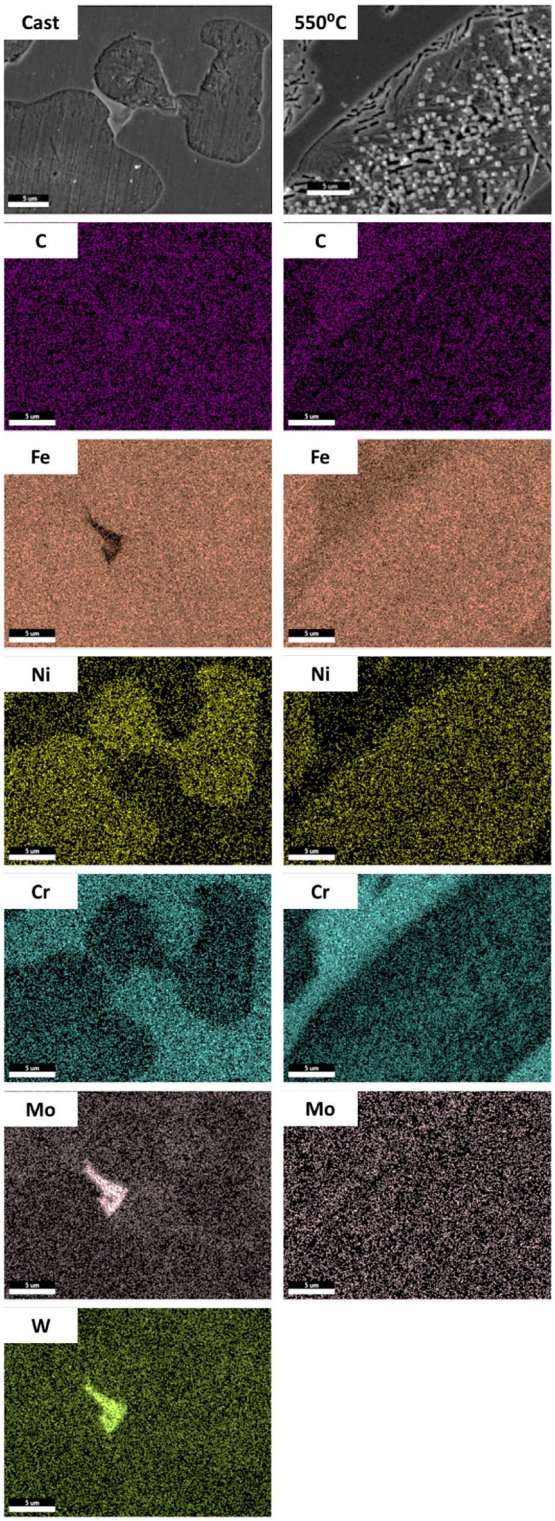


Figure 14. SEM mapping analysis of as-cast and tempered at 550 °C samples.

The friction coefficients of samples were measured under an applied load of 50 N for a distance of 250 m, as given in Figure 17b. The friction coefficient value in the as-cast sample is in the range of 0.72–0.80. After hardening and tempering, it is observed that the friction coefficient values reduced to the range of 0.60–0.72, and the tempering temperature barely affects the friction coefficient. The friction coefficient values of tempered samples are lower than the as-cast. This change in the friction coefficient can be explained by the transformation of the matrix from austenite to martensite and secondary precipitates formed with tempering. In addition, the amount of primary carbides and/or secondary precipitates present in the structure is the cause of fluctuations in the friction coefficient.

After the wear testing, the test specimens were examined with SEM to evaluate the wear mechanisms and surface damage findings. Figure 18 shows the worn surfaces of the as-cast and tempered samples. The wear tracks with grooves parallel to the ball sliding direction are illustrated in Figure 18a–f. Abrasive wear is the primary wear mechanism in two specimen circumstances. Micro-cracking, delamination, and plowing are part of the wear process, as shown in Figure 18. Researchers[39,45–47] have reported similar results. During the test, the particles that were separated from weakly confined carbides by matrix caused abrasive wear. The sample tempered at 550 °C with the highest wear resistance showed micro-cracking and delamination at the wear surface as seen in Figure 18e, but it has less plastic deformation and plowing compared to those of other specimens.

Conclusions

In this study, we investigated the influence of tempering on the microstructure, hardness, and wear resistance of high-alloy WCI (Ni-Hard 4) alloyed with B and W. The obtained results can be summarized as follows:

- Equilibrium and non-equilibrium using Scheil–Gulliver model calculations were performed with Thermo-Calc software. The Scheil–Gulliver model predicted a solidification path involving M_7C_3 carbide precipitation before austenite formation, along with the presence of $M_{23}C_6$ and MC carbides and M_2B_C16 boride. In contrast, the equilibrium path showed a narrower solidification interval, starting with primary M_7C_3 carbide and continuing to austenite and $M_{23}C_6$ carbide

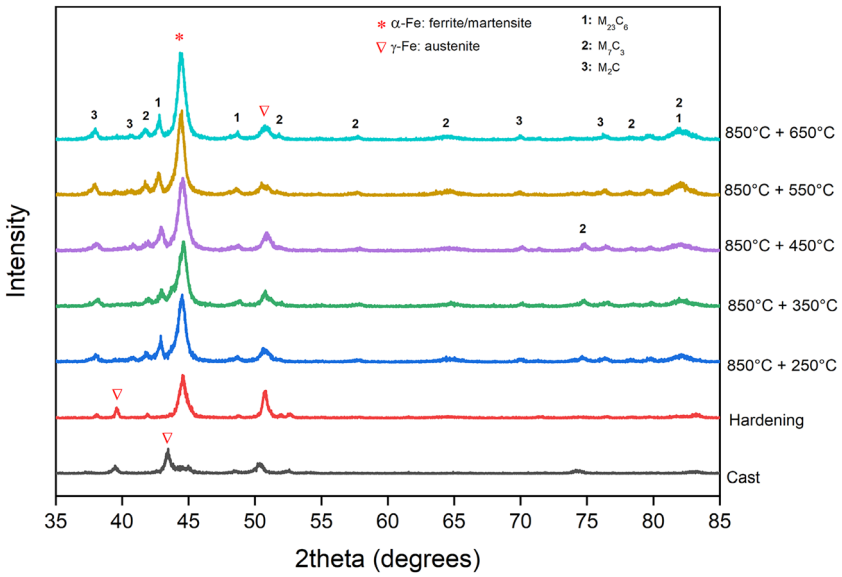


Figure 15. XRD results of the samples in as-cast and tempered conditions.

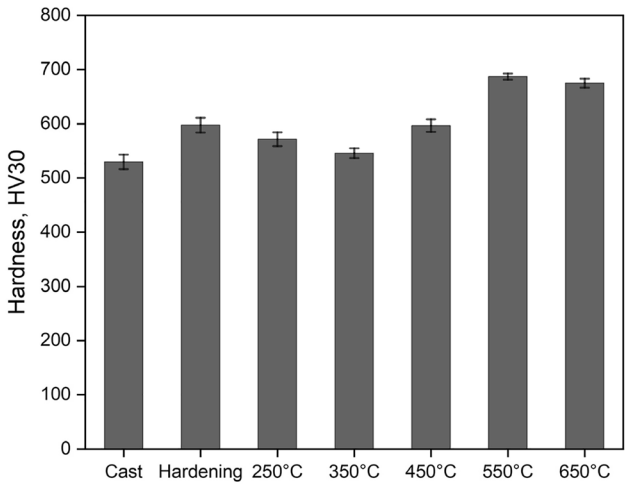


Figure 16. Hardness measurements of samples.

formation. After the microstructural investigations, it was observed that the microstructure of the as-casted sample is close to non-equilibrium conditions.

- Microstructural characterization of the sample in as-casted condition showed that an austenite matrix appeared along primary and eutectic carbides such as M_7C_3, $M_{23}CB_6$ and, M_2CB carbides/carborides. Martensite matrix including secondary carbides observed after the hardening and tempering. It was observed that the amount of secondary carbides increased at tempering temperatures above 550 °C.
- As expected, the hardness increased after hardening and tempering compared to the as-casted condition. Furthermore, an increase in hardness was observed with an increase in tempering temperature. It was attributed to the transformation of austenite to martensite and the precipitation of secondary carbides and carborides.

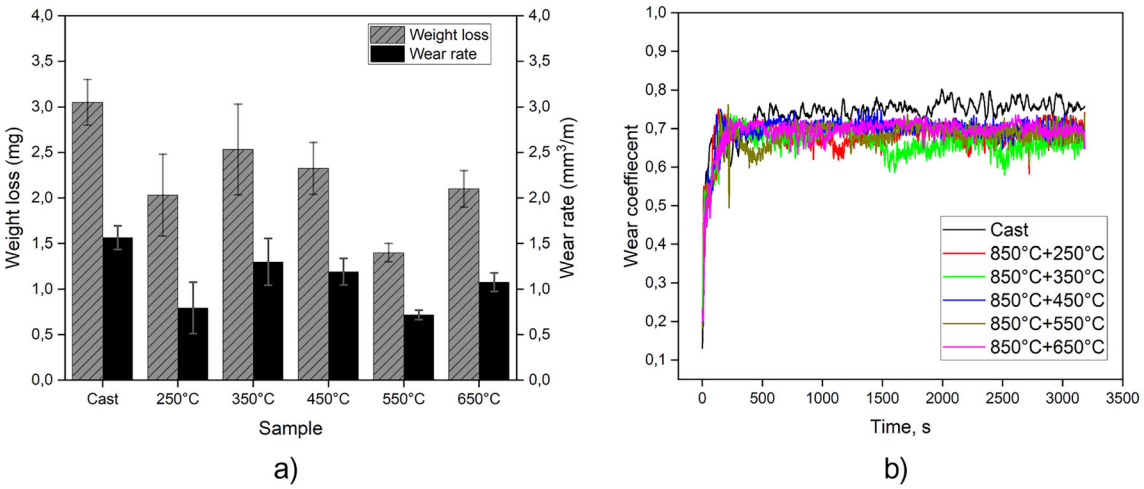


Figure 17. The results of wear testing of the samples in as-casted and tempered conditions: (a) wear rate and weight loss values and (b) coefficient of friction.

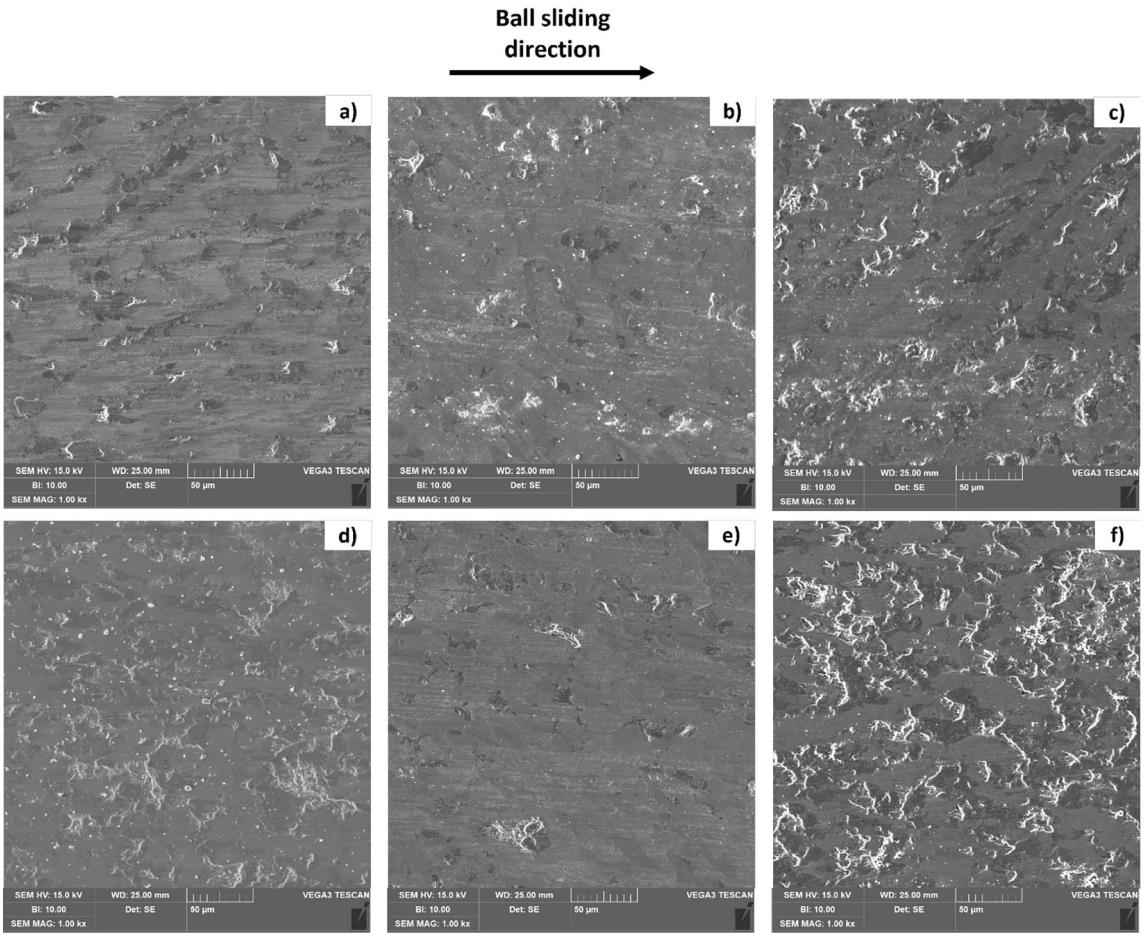


Figure 18. SEM micrographs of worn surfaces high magnification (a) as-cast (b) 250 °C (c) 350 °C (d) 450 °C (e) 550 °C and (f) 650 °C.

- The wear characterization revealed that the number of the grooves due to plowing with plastic deformation decreased after the tempering compared with the sample in as-casted condition. It was found that the optimum tempering temperature is 550 °C depending on the hardness and wear tests performed after the hardening and tempering processes of tungsten-boron aided Ni-Hard 4 material.
- In the wear testing results, abrasive wear was identified as the primary mechanism, with microcracking and delamination observed in the sample tempered at 550 °C. Friction coefficient values decreased after hardening and tempering, with the lowest values recorded for the sample tempered at 350 °C.

Acknowledgements

This research was financially supported by Kocaeli University Research Founder research project number 2018/74.

Funding

Open access funding provided by the Scientific and Technological Research Council of Türkiye (TÜBITAK).

Open Access

This article is licensed under a Creative Commons Attribution 4.0 International License, which permits use, sharing, adaptation, distribution and reproduction in any medium or format, as long as you give appropriate credit to the original author(s) and the source, provide a link to the Creative Commons licence, and indicate if changes were made. The images or other third party material in this article are included in the article's Creative Commons licence, unless indicated otherwise in a credit line to the material. If material is not included in the article's Creative Commons licence and your intended use is not permitted by statutory regulation or exceeds the permitted use, you will need to obtain permission directly from the copyright holder. To view a copy of this licence, visit http://creativecommons.org/licenses/by/4.0/.

REFERENCES

1. M. Mohammadnezhad, V. Javaheri, M. Shamanian, M. Naseri, M. Bahrami, Effects of vanadium addition on microstructure, mechanical properties and wear resistance of Ni-Hard4 white cast iron. Mater. Des. **49**, 888–893 (2013)
2. M. Günay, E. Yücel, Application of Taguchi method for determining optimum surface roughness in turning of high-alloy white cast iron. Measurement **46**(2), 913–919 (2013)
3. A. Sanchez-Cruz, A. Bedolla-Jacuinde, F.V. Guerra, I. Mejía, Microstructural modification of a static and dynamically solidified high chromium white cast iron alloyed with vanadium. Res. Mater. **7**, 100114 (2020)
4. S.G. Banadkouki, S. Mehranfar, H.K. Zarchi, Effect of Cu addition on hardness and microstructural features of low alloy white cast iron. Mater. Res. Express **6**(2), 026547 (2018)
5. Y.P. Wang, D.Y. Li, L. Parent, H. Tian, Improving the wear resistance of white cast iron using a new concept–high-entropy microstructure. Wear **271**(9–10), 1623–1628 (2011)
6. J. Yoganandh, S. Natarajan, S.K. Babu, Erosive wear behavior of nickel-based high alloy white cast iron under mining conditions using orthogonal array. J. Mater. Eng. Perform. **22**, 2534–2541 (2013)
7. ASTM A 532-Standard specification for abrasion resistant cast iron, (1999)
8. M.K. Vidyarthi, A.K. Ghose, I. Chakrabarty, Effect of deep cryogenic treatment on the microstructure and wear performance of Cr–Mn–Cu white cast iron grinding media. Cryogenics **58**, 85–92 (2013)
9. S.R. Al-Sayed, A.M. Elshazli, A.H.A. Hussein, Laser surface hardening of Ni-hard white cast iron. Metals **10**(6), 795 (2020)
10. M. Çöl, F.G. Koç, H. Öktem, D. Kır, The role of boron content in high alloy white cast iron (Ni-Hard 4) on microstructure, mechanical properties and wear resistance. Wear **348**, 158–165 (2016)
11. L. Jinzhu, L. Shizhuo, M. Yongfa, Wear resistance of Ni-hard 4 and high-chromium cast iron re-evaluated. Wear **166**(1), 37–40 (1993)
12. M. Filipovic, E. Romhanji, Z. Kamberovic, Chemical composition and morphology of M7C3 eutectic carbide in high chromium white cast iron alloyed with vanadium. ISIJ Int. **52**(12), 2200–2204 (2012)
13. H. Berns, A. Fischer, Microstructure of Fe-Cr-C hardfacing alloys with additions of Nb. Ti and B. Metallogr. **20**(4), 401–429 (1987)
14. S.M. Anijdan, A. Bahrami, N. Varahram, P. Davami, Effects of tungsten on erosion–corrosion behavior of high chromium white cast iron. Mater. Sci. Eng. A **454**, 623–628 (2007)
15. S.M. Tomovic-Petrovic, S.V. Markovic, S. Zec, The effect of boron on the amount and type of carbides in chromium white irons. J. Serb. Chem. Soc. **67**(10), 697–707 (2002)
16. A.S. Jain, H. Chang, X. Tang, B. Hinckley, M.X. Zhang, Refinement of primary carbides in hypereutectic high-chromium cast irons: a review. J. Mater. Sci. **56**(2), 999–1038 (2020)
17. M. Ngqase, X. Pan, An overview on types of white cast irons and high chromium white cast irons, in Journal of Physics: Conference Series, Vol. 1495, No. 1 (IOP Publishing, 2020) p. 012023

18. K.S. Al-Rubaie, M. Pohl, Heat treatment and two-body abrasion of Ni-Hard 4. Wear **312**(1–2), 21–28 (2014)
19. A. Bedolla-Jacuinde, L. Arias, B. Hernández, Kinetics of secondary carbides precipitation in a high-chromium white iron. J. Mater. Eng. Perform. **12**(4), 371–382 (2003)
20. X. Jia, Q. Hao, X. Zuo, N. Chen, Y. Rong, High hardness and toughness of white cast iron: the proposal of a novel process. Mater. Sci. Eng. A **618**, 96–103 (2014)
21. A. González-Pociño, J. Asensio-Lozano, F. Álvarez-Antolín, A. García-Diez, Evaluation of hardness, sliding wear and strength of a hypoeutectic white iron with 25% Cr after heat treatments. Metals **11**(6), 947 (2021)
22. C.P. Tabrett, I.R. Sare, M.R. Ghomashchi, Microstructure-property relationships in high chromium white iron alloys. Int. Mater. Rev. **41**(2), 59–82 (1996)
23. J.P. Lai, Q.L. Pan, Y.W. Sun, C.A. Xiao, Effect of Si content on the microstructure and wear resistance of high chromium cast iron. Isij Int. **58**(8), 1532–1537 (2018)
24. M.M. Mourad, S. El-Hadad, M.M. Ibrahim, Effects of molybdenum addition on the microstructure and mechanical properties of ni-hard white cast iron. Trans. Indian Inst. Met. **68**(5), 715–722 (2015)
25. A. Bedolla-Jacuinde, R. Correa, J.G. Quezada, C. Maldonado, Effect of titanium on the as-cast microstructure of a 16% chromium white iron. Mater. Sci. Eng. A **398**(1–2), 297–308 (2005)
26. Y. Lv, Y. Sun, J. Zhao, G. Yu, J. Shen, S. Hu, Effect of tungsten on microstructure and properties of high chromium cast iron. Mater. Des. **39**, 303–308 (2012)
27. M. Kang, Y. Suh, Y.J. Oh, Y.K. Lee, The effects of vanadium on the microstructure and wear resistance of centrifugally cast Ni-hard rolls. J. Alloy. Compd. **609**, 25–32 (2014)
28. A. Bedolla-Jacuinde, Microstructure of vanadium-, niobium-and titanium-alloyed high-chromium white cast irons. Int. J. Cast Met. Res. **13**(6), 343–361 (2001)
29. A.N. Sudhakar, R. Markandeya, K.P. Ajoy, D. Kaushik, Effect of alloying elements on the microstructure and mechanical properties of high chromium white cast iron and Ni-Hard iron. Mater. Today: Proc. **61**, 1006–1014 (2022)
30. Z. Liu, Y. Li, X. Chen, K. Hu, Microstructure and mechanical properties of high boron white cast iron. Mater. Sci. Eng. A **486**(1–2), 112–116 (2008)
31. R. Correa, A. Bedolla-Jacuinde, J. Zuno-Silva, E. Cardoso, I. Mejía, Effect of boron on the sliding wear of directionally solidified high-chromium white irons. Wear **267**(1–4), 495–504 (2009)
32. H. Kazdal Zeytin, H. Yildirim, B. Berme, S. Duduoĝlu, G. Kazdal, A. Deniz, Effect of boron and heat treatment on mechanical properties of white cast iron for mining application. J. Iron. Steel Res. Int. **18**(11), 31–39 (2011)
33. N. Saunders, A.P. Miodownik (eds.), *CALPHAD (Calculation of Phase Diagrams): A Comprehensive Guide* (Elsevier, 1998)
34. ASTM G99-17, Standard test method for wear testing with a pin-on-disc apparatus, ASTM International, West Conshohocken, PA, (2017), www.astm.org
35. R.H. Purba, K. Shimizu, K. Kusumoto, Y. Gaqi, T. Todaka, Effect of boron addition on three-body abrasive wear characteristics of high chromium based multi-component white cast iron. Mater. Chem. Phys. **275**, 125232 (2022)
36. X. Chen, Y. Li, Effect of heat treatment on microstructure and mechanical properties of high boron white cast iron. Mater. Sci. Eng. A **528**(2), 770–775 (2010)
37. E. Cortés-Carrillo, A. Bedolla-Jacuinde, I. Mejía, C.M. Zepeda, J. Zuno-Silva, F.V. Guerra-Lopez, Effects of tungsten on the microstructure and on the abrasive wear behavior of a high-chromium white iron. Wear **376**, 77–85 (2017)
38. S. Ma, J. Zhang, Wear resistant high boron cast alloy—a review. Rev. Adv. Mater. Sci. **44**(1), 54–62 (2016)
39. Z.L. Liu, C. Xiang, Y.X. Li, K.H. Hu, High boron iron-based alloy and its modification. J. Iron. Steel Res. Int. **16**(3), 37–54 (2009)
40. M.A. Guitar, S. Suárez, O. Prat, M. Duarte Guigou, V. Gari, G. Pereira, F. Mücklich, High chromium cast irons: destabilized-subcritical secondary carbide precipitation and its effect on hardness and wear properties. J. Mater. Eng. Perform. **27**, 3877–3885 (2018)
41. A. Bedolla-Jacuinde, F.V. Guerra, A.J. Guerrero-Pastran, M.A. Sierra-Cetina, S. Valdez-Medina, Microstructural effect and wear performance of high chromium white cast iron modified with high boron contents. Wear **476**, 203675 (2021)
42. M. Jokari-Sheshdeh, Y. Ali, S.C. Gallo, W. Lin, J.D. Gates, Comparing the abrasion performance of NiHard-4 and high-Cr-Mo white cast irons: the effects of chemical composition and microstructure. Wear **492**, 204208 (2022)
43. K. Ruangchai, R. Tongsri, J.T.H. Pearce, T. Chairuangsri, A. Wiengmoon, Effects of annealing treatment on microstructure and hardness in the 28 wt% Cr cast iron with Mo/W addition. J. Metals Mater. Miner. **31**(2), 89–95 (2021)
44. K. Rohrig, Ni-Hard Material Data and Applications, Nickel Development Institute, Technology & Engineering, Toronto, (1996), pp. 1–28
45. R.J. Chung, X. Tang, D.Y. Li, B. Hinckley, K. Dolman, Microstructure refinement of hypereutectic high Cr cast irons using hard carbide-forming elements for improved wear resistance. Wear **301**(1–2), 695–706 (2013)

46. J.J. Coronado, Effect of load and carbide orientation on abrasive wear resistance of white cast iron. Wear **270**(11–12), 823–827 (2011)
47. A.N. Sudhakar, R. Markandeya, B.S. Rao, A.K. Pandey, D. Kaushik, Effect of alloying elements on the dry sliding wear behavior of high chromium white cast iron and Ni-hard iron. Mater. Today Proc. **60**, 1303–1309 (2022)

Publisher's Note Springer Nature remains neutral with regard to jurisdictional claims in published maps and institutional affiliations.